E-NEWSLETTER

December 2020 issue

THE SOCIETY OF ACOUSTICS SINGAPORE

Official Address: 33 Oxford Road, #04-03, Kentish Court, Singapore 218816, Singapore.
Tel: 62990485 and Mobile No. 90932730 Fax: 62990485

E-mail: wsgan@metaultrasound.com
Website: www.acousticssingapore.com

Registration No: 0331/1989
Year of Registration: 1989

CONTENTS

I.CONFERENCE NEWS

. The 27^{7h} International Congress on Sound and Vibration(ICSV27) will be held in Prague.Czech Republic from 11 to 15 July 2021.

Woon Siong Gan will be organising three structured sessions on:

1. Nonlinear acoustics and vibration
2. Acoustic metamaterials & phononic crystals: fundamentals and applications
3. Sound propagation in curvilinear spacetime

Please visit www.icsv27.org for more informations.

Due to the coronavirus situation, the ICSV27 will be postponed to 11 to 15 July 2021, but will still be held at the same hotel in Prague. Please visit www.icsv27.org for further informations.

II.ANNONCEMENTS

The Society of Acoustics will be sending out invoices to members with outstanding membership subscriptions. Members are encouraged to make payment in support of the Society.

The E-Newsletters will be made available to industrial contacts in an effort to promote the activities of the Society.

The Society is also exploring the possibility of organising talks and other professional events in collaboration with acoustic societies of other countries.

Membership Certificates will soon be made available to all members who had made full payments of membership dues

The Society aims to increase membership by inviting all persons, including those from the institution of higher learning and other related societies such as the Institute of Architects, Singapore and the members of the mechanical engineering division of the Institution of Engineers, Singapore who are qualified in the various field of Acoustics to join our Society.

We are especially keen to invite students to join our society and we are establishing the Youth Chapter soon.

III.INTERNATIONAL ACOUSTICS NEWS

Woon Siong Gan was recently elected as a Director of the International Institute of Acoustics and Vibration(IIAV) for the period 2018 to 2022.

MINUTES OF THE ICA GENERAL ASSEMBLY

Tuesday 03 November 2020

11:00 to 12:00 CET

Virtual Meeting

(scrutiny of the votes of the online consultation)

In attendance (online consultation by email): Mark Hamilton (ICA President), Jeong-Guon Ih (ICA Vice-

President), Michael Taroudakis (ICA Past President), Martin Ochmann (ICA Treasurer), Antonino Di

Bella (ICA Secretary-General);

Member Society appointed representatives (online/email vote): Nilda Vechiatti (Argentina), Marion

Burgess (Australia), Dominique Pleeck (Belgium), Bruno Masiero (Brazil), Jérémie Voix (Canada),

David Parra (Chile), Fenghua Li (China), Tino Bucak (Croatia), Panu Maijala (Finland), Jean-

Dominique Polack (France), Jesko Verhey (Germany), Michael Taroudakis (Greece), William Fung

(Hong Kong), Beáta Mesterházy (Hungary), Mahavir Singh (India), Antonino Di Bella (Italy), Akinori

Ito (Japan), Jeong-Guon Ih (Korea), Kyogu Lee (Korea), Sung-Hwan Shin (Korea), James Whitlock

(New Zealand), Jorge Moreno (Peru), Grazyna Grelowska (Poland), Jorge Patrício (Portugal), Woon

Siong Gan (Singapore), Monika Rychtarikova (Slovakia), Mateja Dovjak (Slovenia), Antonio Pedrero

(Spain), Kurt Eggenschwiler (Switzerland), Ayca Sentop-Dumen (Turkey), Jo Webb (United

Kingdom);

International Affiliate appointed representatives (online/email vote): Manell Zakharia (EAA), Nilda

Vechiatti (FIA), Mathias Basner (ICBEN), Sigrun Hirsekorn (ICU), Marion Burgess (I-INCE),

Patricia Davies (USA-INCE).

Note that these minutes, complete with the supporting attachments and other documents referenced, are

posted at the internal Board archive. Only the minutes are posted on the public webpage at

www.icacommission.org/minutes.html.

1. Opening of the Meeting

The 2020 ICA General Assembly was held “virtually” by means of an electronic consultation on the

deliberations of the annual Board Meeting (15-16/07/2020).

Consultation procedures were prepared by the Executive Officers, as resolved during the Board

Meeting, and sent to all the Member Society and International Affiliates. The Secretary-General was

appointed as moderator of the whole procedure.

The appointment of the delegates was made by filling in an online form from 02/10/2020 to

16/10/2020.

Online vote, by filling in an online form or by email, was opened on 19/10/2020 and closed on

02/11/2020.

The scrutiny was carried out on 03/11/2020 by the Secretary-General and results checked by the

Executive Officers.

2. Approval of the Agenda

No changes to the agenda were requested during the online consultation and the agenda was

approved.

3. Election of the Chairperson for the Meeting

As for ordinary assemblies, Secretary-General Antonino Di Bella noted that it was typical to elect

the ICA President to chair the General Assembly. This was implicit in the online consultation.

4. Quorum

Secretary-General Antonino Di Bella confirmed that the quorum, which according to the ICA

Statutes is required for the decisions to be made, has been achieved. In particular, the two

requirements for a properly constitute assembly were fulfilled: more than half of those having the

right to vote (35 Members and International Affiliate on a threshold 27) and more than half of the

maximum number of official delegates (83 Delegates on a threshold of 62) participated in the

consultation.

Overall, 160 out of 223 shares (71.7%) were represented.

Two Members (India and Korea) chose to be represented individually by their Delegates (one

Delegate, one vote). All other Members have chosen to be represented collectively (only one Delegate

was appointed as a representative and his/her vote was multiplied by the number of votes assigned

to the Member).

5. Financial Statement and Budget 2019-2020

The Balance Sheet 2019-2020, the Provisional Budget, and the IYS Global Budget.

were approved unanimously (83 votes in favour, no abstentions, no opposed).

6. ICA Internal Regulations changes

Changes in Internal Regulation Article 4 "The ICA General Assembly" in accordance with the

requirements specified by the Spanish authorities (country of ICA registration) were approved

unanimously (83 votes in favour, no abstentions, no opposed).

7. Membership - Changes in shares

SOBRAC's request to reduce the number of shares from 4 to 1 was approved with a two-thirds

majority (77 votes in favour, 6 abstentions, no opposed).

8. Membership - Application for membership

AAVI (Indonesia) application for full ICA Member with one share was approved unanimously (83

votes in favour, no abstentions, no opposed).

9. Adjourn

President Mark Hamilton closed the 2020 ICA General Assembly thanking all the Board members

for their contribution to the ICA Administration as well as all the Members and International

Affiliates for their collaboration and their support to the ICA activities.

IV.MEMBERSHIP SUBSCRIPTION

Fellow	S$70
Member	S$50
Associate	S$30
Student	S$15
Corporate	S$200

FEE BASED ON ANNUAL RATE

FOR MORE INFORMATION PLEASE CONTACT: Dr. Woon Siong Gan at
email: wsgan5@gmail.com

Membership application forms can be downloaded from the society website: www.acousticssingapore.com. Please complete and email to wsgan5@gmail.com

Microfluidics and Nanofluidics (2020) 24:92
https://doi.org/10.1007/s10404-020-02397-5

RESEARCH PAPER

Acoustophoretic agglomeration patterns of particulate phase in a host fluid

Shahrokh Sepehrirahnama[1] · **Kian-Meng Lim**[2]

Received: 24 June 2020 / Accepted: 10 October 2020

Abstract
Ultrasound-assisted processing of particulate phase in a host fluid relies on the induced acoustic force field. Understanding the agglomeration phenomenon in the particulate phase under acoustic forces will provide better insight about the acoustophoresis quality and a way to design a well-controlled process. In this work, a dynamic model consisting of acoustic and hydrodynamic forces is proposed for tracking the motion of micro-spheres under ultrasound fields with planar and non-planar wave fronts. The agglomeration of particles at the nodal plane was simulated taking into account the contact and collisions between spheres. The numerical simulations were conducted for both sound hard and compressible spheres to investigate the behaviors of single and multiple-phase particle populations. For the case of a plane standing-wave, the interaction between solid-bubble allows the solid particles to stay at the velocity node which is their unstable equilibrium location. With a Bessel standing wave as a non-planar pressure field, the agglomeration patterns of particles are generally different from the case of plane standing wave, which implies the significance of the particle tracking simulations for predicting the agglomeration patterns and locations under ultrasound fields with arbitrary wave fronts.

Keywords Ultrasound particle manipulation · Acoustofluidics · Acoustic Radiation Force · Bessel Standing Wave · Bubble-Solid interaction

1 Introduction

Ultrasound has been used for manipulation of suspended micro-particles such as gas bubbles, liquid droplets, biological cells and solid particles in a host fluid (Augustsson et al. 2012; Hartono et al. 2011; Tiong et al. 2019; Mishra et al. 2014; Wijaya et al. 2016; Ma et al. 2017; Xuan et al. 2010). Compared to other particle manipulation techniques such as dielectrophoresis and magnetophoresis, ultrasound allows manipulating all particles at once in a label-free manner. The underlying physics of ultrasound particle manipulation is the acoustic radiation force (Augustsson et al. 2012; Settnes and Bruus 2012; Doinikov 1994a, b; Wiklund et al. 2012; Hartono et al. 2011; Garcia-Sabaté et al. 2014; Mohapatra et al. 2018). This force is derived from nonlinear stresses due to the interaction between incident and scattering fields, time-averaged over a wave cycle (Settnes and Bruus 2012; Doinikov 1994a, b; Sepehrirahnama et al. 2015a, b). Each particle in a sound field is subjected to the primary radiation force that is the result of interaction between the external incident field and particle's scattered field. The secondary radiation force, also known as acoustic interaction force, is present in close proximity to other particles that is due to the interactions between scattered fields of multiple particles (Sepehrirahnama et al. 2015a, b; Doinikov 2001, 2002; Silva and Bruus 2014).

Depending on the material properties, primary radiation force pushes particles to certain locations in a sound field, such as pressure or velocity nodes in a standing wave. This phenomenon was adapted in devising manipulation processes such as particle separation and sorting on micro- fluidic chips (Augustsson et al. 2012; Mishra et al. 2014; Wijaya et al. 2016; Wiklund et al. 2012; Hartono et al. 2011; Mohapatra et al. 2018; Wiklund 2012). However, particles experience the secondary force which determines their mode of agglomeration (Mohapatra et al. 2018;

✉ Shahrokh Sepehrirahnama
Shahrokh.sepehrirahnama@uts.edu.au

[1] Centre for Audio, Acoustics and Vibration (CAAV), University of Technology Sydney, Sydney, NSW 2007, Australia

[2] Mechanical Engineering Department, National University of Singapore, Singapore 117575, Singapore

Published online: 02 November 2020

Sepehrirahnama et al. 2015a, b; Silva and Bruus 2014; Lopes et al. 2016; Zhang and Li 2016; Tiong et al. 2019; Feng et al. 2020). Thus, designing ultrasound-powered particle manipulators would require consideration of both primary and secondary forces, factoring in the distribution of particles and their positions.

Study of the acoustical bubble-bubble and bubble-solid interactions in a mixed population of particles were reported to shed light on the agglomeration patterns under an ultrasound field (Doinikov 1999, 2001, 2002; Doinikov et al. 2016; Feng et al. 2020; Shang et al. 2016). However, those studies were limited to the interaction between a pair of particles with an axisymmetric arrangement with respect to the wave direction, while focusing on the changes in the interaction forces. Although such studies are insightful, further work is required to correctly predict the motion of particles in an acoustic field (Sepehrirhnama and Lim 2020), which can be used in designing efficient ultrasound-assisted particle manipulations.

Particle agglomeration in a sound field can be simulated by accounting for the forces acting on each and every particle (Chen et al. 2020; Vyas et al. 2019; Devendran et al. 2014; Lei 2017). For self-buoyant particles, these are acoustic and hydrodynamic forces (Garcia-Sabaté et al. 2014; Mohapatra et al. 2018; Lei 2017). Moreover, particles experience multiple collisions during the clustering process. This needs to be accounted for to predict the final configuration of their aggregate. A suitable time-marching algorithm based on particle dynamics and an appropriate collision detection model will serve as a potential choice for theoretical simulation of such particle agglomeration.

The acoustic forces primarily depend on the incident field. Plane standing wave has been studied as a practical choice for ultrasound manipulation. It was reported that the primary acoustic force due to a standing wave is significantly larger than that of a plane traveling wave of this magnitude (Settnes and Bruus 2012; Doinikov 1994a, b). Another choice of incident wave is a standing Bessel beam that is a standing wave along the beam axis and a zeroth order Bessel function in the transverse direction (Marston et al. 2006; Marston 2006, 2007; Zhang and Marston 2011; Mitri 2015; Wijaya and Lim 2016). Theoretically, this nonplanar incident wave can be constructed using a series of plane wave sources arranged in a circular configuration with their wave vectors passing through the axis [9-12]. For travelling Bessel beam, the pull-in effect has been reported for a single particle that is positioned along the beam axis and where its size-to-wavelength ratio falls in a certain range (Marston et al. 2006; Marston 2006, 2007; Zhang and Marston 2011; Mitri 2015; Wijaya and Lim 2016). However, the effects of a standing Bessel beam on a population of particles needs to be investigated, especially in the Rayleigh size limit, $ka \ll 1$ with k being the wave number and a denoting the nominal size of particles.

In this work, we present a simple and straightforward time-marching algorithm for tracking spherical particles under acoustic radiation and hydrodynamic drag to simulate their clustering in a sound field. In this algorithm, particle collision is accounted for automatically that allows particles to stick to each other or get separated during their journey from their initial position to the final resting position. For solving the multi-scattering problem, we use the multipole series expansion, also known as partial-wave expansion, that is suitable for simulating spherical particles. Our numerical results show the applicability of the time-marching algorithm in terms of simulating the physics of particle agglomeration for an arbitrary number of particles. Such simulation tool finds applications in modelling and predicting the behavior of particulate phases during industrial processes such as decontamination of fluids or synthesis of polymeric particles.

2 Theory of acoustic forces and particle tracking

The governing equation of acoustic fields is

$$\nabla^2 \emptyset = \frac{1}{c^2} \frac{\partial^2 \emptyset}{\partial t^2}, \tag{1}$$

where $\emptyset$ denotes the velocity potential, t denotes time, c is the speed of sound in the fluid medium, and $\nabla_2 = \nabla \cdot \nabla$. Acoustic pressure P and velocity _ are obtained from the velocity potential $\emptyset$ as follows:

$$P = -\rho \frac{\partial \emptyset}{\partial t} \tag{2}$$
$$v = \nabla \emptyset$$

2.1 Incident field and multiple scattering

For the case of N particles in a fluid, the velocity potential $\emptyset$ is written as

$$\emptyset = \emptyset_0 + \sum_{l=1}^{N} \emptyset_l \tag{3}$$

where $\emptyset_0$ denotes the incident field potential and $\emptyset_l$ is the scattered field potential from the lth particle. These potentials are expressed using the partial wave expansion as follows:

$$\emptyset_0 = e^{-i\omega t} \sum_{p=0}^{\infty} \sum_{q=-p}^{p} A_{pq} j_p(kr) Y_{pq}(\theta, \varphi) \quad (4)$$

$$\emptyset_l = e^{-i\omega t} \sum_{p=0}^{\infty} \sum_{q=-p}^{p} B_{pq}^{(l)} h_p(kr_l) Y_{pq}(\theta_l, \varphi_l),$$

where ω is the circular frequency, $(r_l, \theta_l, \varphi_l)$are the spherical coordinates with respect to the center of the *l*th sphere, *j* and *h* are spherical Bessel function and Hankel function of the first kind of degree p, respectively, Y_{pq} denotes spherical harmonics of degree p and order q Doinikov 1994a, b), A_{pq} and $B_{pq}^{(l)}$ denote the constant coefficients, and $i = \sqrt{-1}$. Similarly, the refracted potential field inside the *l*th particle is written as

$$\emptyset_l = e^{-i\omega t} \sum_{p=0}^{\infty} \sum_{q=-p}^{p} C_{pq}^{(l)} j_p(k_l r_l) Y_{pq}(\theta_l, \varphi_l), \quad (5)$$

where $C_{pq}^{(l)}$ denotes the coefficients of the refracted field potential, and $k_l = \frac{\omega}{c_l}$ with c_l being the speed of sound inside particle *l*. For a given incident wave, we assume that A_{pq} are known for the time being. The expressions for A_{pq} are discussed in the following subsections 2.1.1 to 2.1.2. Coefficients $B_{pq}^{(l)}$ and $C_{pq}^{(l)}$ are obtained by imposing the boundary conditions (Yosioka and Kawasima 1955; Doinikov 1994a,b) on the surface of the *l*th sphere $r_l = a_l$,

$$v_0 \cdot n_l + \sum_{q=0}^{N} v_q \cdot n_l = v_l^R \cdot n_l + u_l \cdot n_l \quad (6)$$

$$P_0 + \sum_{q=0}^{N} P_q = P_l^R,$$

where a_l and u_l denote the radius and rigid-body oscillation velocity of the *l*th particle, respectively, and **n** is the unit outward-normal vector. For the case of rigid spheres, the internal wave refraction is absent, $C_{pq}^{(l)} = 0$, and normal velocity condition will give the unknown scattering coefficients $B_{pq}^{(l)}$. This multi-scattering problem of *N* spheres with arbitrary arrangement can be solved numerically (Sepehrirahnama et al. 2015a, b; Doinikov 2001; Lopes et al. 2016).

2.1.1 Plane Standing Wave

The incident potential for a plane standing wave along the *z*-axis is given as follows

$$\emptyset_0 = A\cos\big(k(z + h_z)\big), \quad (7)$$

where *A* denotes the magnitude of the wave, h_z is the distance in the *z* direction between the nearest velocity node and the center of expansion. Using the plane wave expansion, coefficients A_{pq} become (King 1934; Doinikov 1994a,b)

$$A_{pq} = 4\pi A\left[e^{ikh_z} + (-1)^P e^{-ikh_z}\right] i^P \delta^{q0} \quad (8)$$

where δ^{q0} denotes the Kronecker delta that is unity for $q = 0$ and zero otherwise.

2.1.2 Bessel standing wave

For a Bessel standing wave with axis along the *z* direction,
the incident potential is expressed as

$$\emptyset_0 = AJ_0\big(kRsin(\beta)\big)cos\big(kcos(\beta)(z + h_z)\big) \quad (9)$$

where J_0 denotes the zero-order cylindrical Bessel function, $R = \sqrt{x^2 + y^2}$ *and* β denotes the cone angle that is angle between the wave vector and *z*-axis. Then, coefficients A_{pq} become

$$A_{pq} = A\sqrt{4\pi(2p+1)}Y_{pq}(\beta, 0)[e^{ikh_z} + (-1)^P e^{-ikh_z}]i^P \delta_{q0} \quad (10)$$

when the center of expansion lies on the Bessel beam axis. For the case of the center being off-axis, the incident coefficients are obtained using multipole translation method, as follow,

$$\bar{A}_{pq} = \sum_{v=0}^{\infty} \sum_{\mu=-v}^{v} T_{pv}^{q\mu} A_{v\mu} \quad (11)$$

where $\bar{A}_{pq}$ denotes the incident coefficients for an off-axis center of expansion, $A_{v\mu}$ are calculated from Eq. (10), $T_{pv}^{q\mu}$ denotes the Regular-to-Regular multipole translation coefficients, whose expressions are obtained from equations (2.7) and (2.8) in reference (Doinikov 2001).

2.2 Particle dynamics

For a fluid with negligible viscosity, acoustic radiation force
acting on the *l*th particle is written as

$$F = \int_{r_l} < \sigma - vv > \cdot n d\Gamma \quad (12)$$

where _*l* denotes surface of the *l*th particle and $\sigma = \frac{\rho}{2} v \cdot v - \frac{1}{2\rho c^2} P^2$ .This integral gives the resultant acoustic force from the primary and secondary radiation forces. This acoustic force is balanced out by hydrodynamic forces as the particles moves through the host fluid. It is noted that the acoustic interaction among the particles through the secondary radiation forces are fully coupled to one another, as the

coefficients of the scattered fields are solved simultaneously.

The hydrodynamic forces, denoted by **H** include the Stokes drag force and the interaction drag force due to the relative motion among the particles. We adapt the proposed model for hydrodynamic forces in reference (Mohapatra et al.2018),

$$\begin{pmatrix} U_1 \\ U_2 \\ \vdots \\ U_N \end{pmatrix} = \frac{1}{6\pi\mu a}\begin{bmatrix} I & C_{12} & \cdots & C_{1N} \\ C_{21} & I & \cdots & C_{2N} \\ \vdots & \vdots & \ddots & \vdots \\ C_{N1} & C_{N2} & \cdots & I \end{bmatrix}\begin{pmatrix} H_1 \\ H_2 \\ \vdots \\ H_N \end{pmatrix},$$

$$C_{jl} = \frac{3a}{4}\left(\frac{I}{r} + \frac{r_{jl}r_{jl}}{r^3}\right) + \frac{a^3}{4}\left(\frac{I}{r^3} - 3\frac{r_{jl}r_{jl}}{r^5}\right), \qquad (13)$$

$$r_{jl} = x_j - x_l,$$

where $\boldsymbol{U}_j$ denotes the translation velocity of particle j in the time scale much larger than the period of one oscillation of the acoustic field, μ is the dynamic viscosity of the fluid, **I** denotes the identity matrix of size 3, $\boldsymbol{x}_j$ is the position vector of the jth sphere and $r = |\boldsymbol{r}_{jl}|$ is the distance between particle j and particle l. The expression of $\boldsymbol{C}_{jl}$ was derived from the Stokeslet theory that relates the velocity at the target point $\boldsymbol{x}_j$ to the applied force $\boldsymbol{H}_l$ at the source point $\boldsymbol{x}_l$ in a fluid domain (Pozrikidis 1992). The fully populated matrix reflects the fully coupled nature of the hydrodynamics interaction among the cluster of particles, similar to the acoustic force interaction. Since the mass of micro-particles is small, the quasi-static condition may be used:

$$\boldsymbol{F}(\boldsymbol{x}) + \boldsymbol{H}(\boldsymbol{U}) \approx \boldsymbol{0} \qquad (14)$$

The acoustic radiation force depends on the location of the particle in the sound field whereas the hydrodynamic force is a function of particles' velocities. Thus, Eq. (14) is a first-order differential equation with respect to time, which can be numerically solved by appropriate time-marching algorithms such as the Euler methods. Collisions among the particles have to be considered while tracking the particles in the sound field. Since all particles are assumed to be spherical, collision occurs when the center-to-center distance of two particles is less than the sum of their radii. To resolve a detected collision, the penetration distance is measured from the displacement of particles in the center-to-center direction at time t. Then, the time step is reduced and the particles are displaced back along their center-to-center direction until their surfaces touch each other. This is obvious for two penetrating spheres. For the case of more than two particles, the same position correcting technique is applied to all particles in a pairwise manner until there are no penetrating particles left, as shown in Fig. 1. Then, we proceed with the force calculations at the next time step $t + \Delta t$ Spheres that are in contact may continue to move together as a single entity maintaining the contact state, or they may move apart or disperse according to the forces acting on each sphere.

3 Results

The tracking of particles in this section were simulated for P = 100 kPa, with water as the host fluid (ρ = 1000 kg/m3, c = 1500 m/s), and compressible particles made of Pyrex (ρ_p/ρ = 2.23 , c_p/c = 3.78), Polystyrene (ρ_p/ρ = 1.05 , c_p/c = 1.57) and air (ρ_p/ρ = 0.001 , c_p/c = 0.229). The wave frequency is set to 1.5 MHz and particle size is 5 μm, resulting in ka = 0.0314 $\ll$ 1. Displacement and position variables are normalized by the wavelength λ. For normalizing the force and time results, we introduce reference force F_0 and time t_0

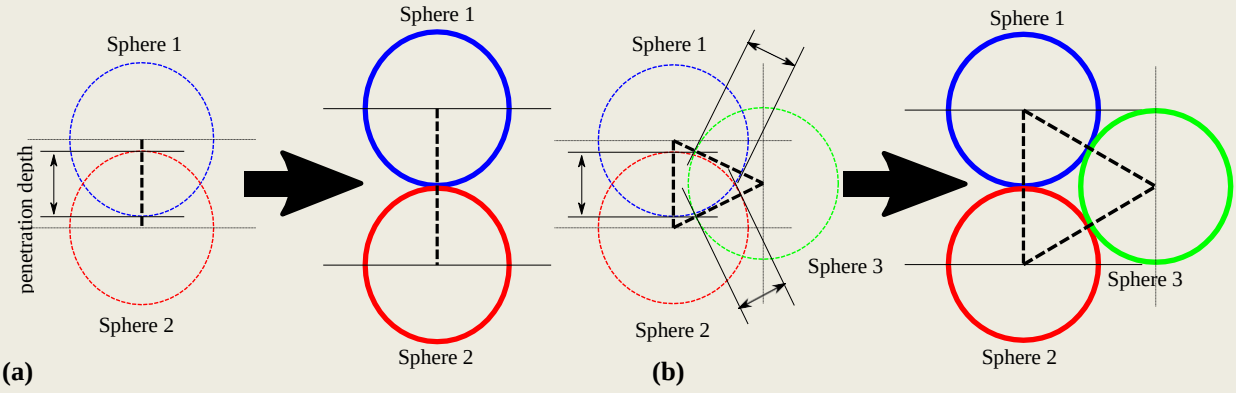

Fig. 1 Applying the position correcting technique for (**a**) two, and (**b**) three penetrating particles

$$F_0 = \pi k a^3 E_0 \quad (15)$$

$$t_0 = \frac{6\pi\mu a\lambda}{F_0}$$

where $E_0 = \frac{1}{4\rho c^2} P^2$ denotes acoustic energy density of the incident wave, and a is the particle radius. For these parameters, the reference force F_0 is equal to 2.74 pN. Considering $\mu = 8.89 \times 10^{-4}$ Pa· s, the reference time t_0 is equal to 30.56s. In the subsequent figures, the trajectories of particles are shown with coloured lines and their initial positions are marked with insets of numeric labels.

3.1 Plane standing wave

3.1.1 Single phase particle population

A plane standing wave along the *z*-direction with pressure node at $z = 0$ is considered for the numerical simulations. First, two particles were traced from their initial positions in the vicinity of the pressure node. The particles are in the *x*-*z* plane, hence there is no force in the *y* direction. Figure 2 shows the trajectories for the two cases of rigid and compressible particles. It is observed that, in both cases, particles travelled from their initial positions towards the pressure node, which is illustrated by a transparent plane at $z = 0$, due to the primary radiation force. There is a sudden deflection in the trajectories, showing that the interaction between the particles becomes stronger at the vicinity of the pressure node.

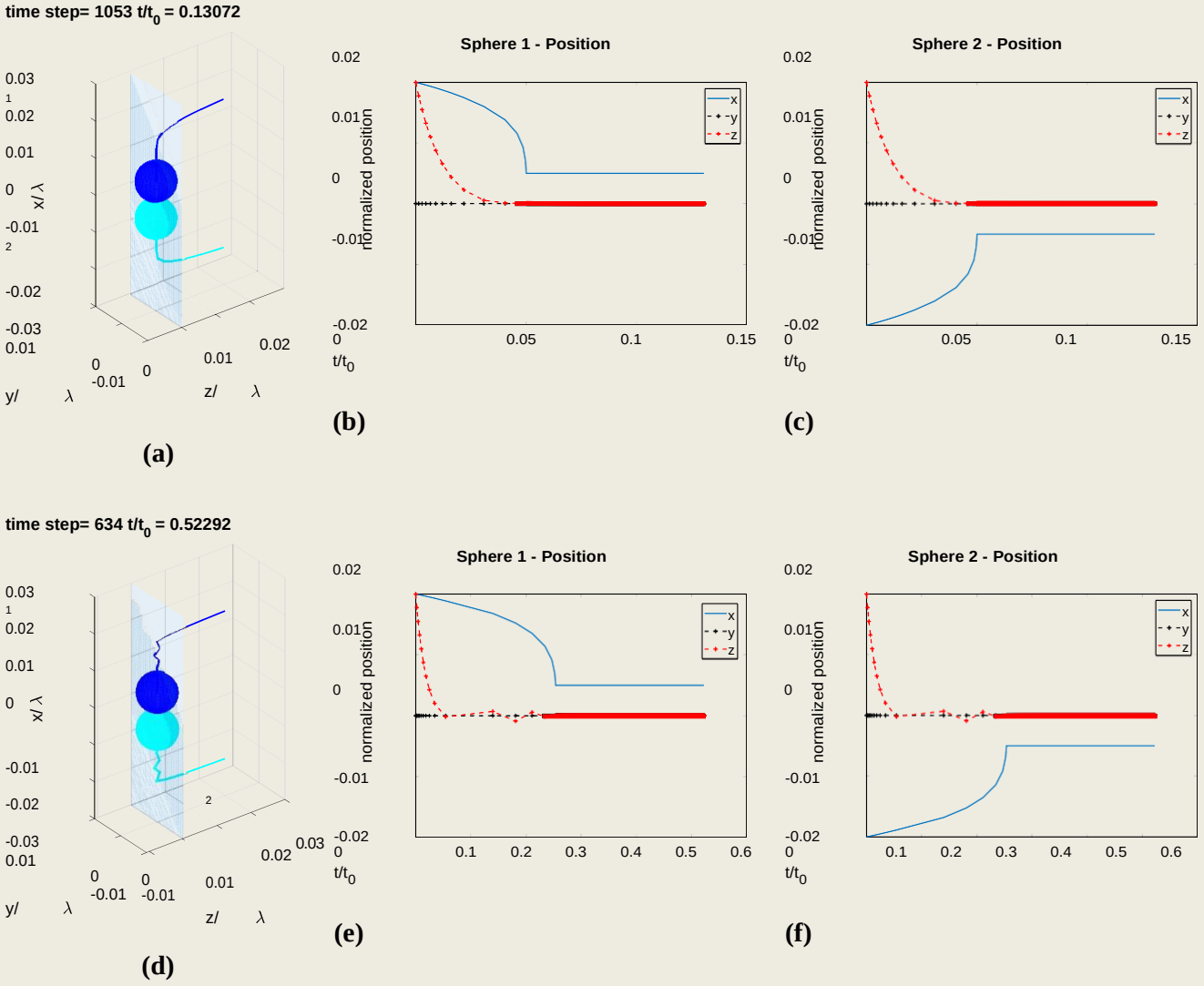

Fig. 2 Trajectories of a pair of (**a**, **b**, **c**) rigid and (**d**, **e**, **f**) compressible particles at the vicinity of pressure node. Normalized position refers to the (*x*, *y*, *z*) for each particle divided by the wavelength *ß*. The simulation time *t* is normalized with respect to t_0, which represents the required time for a particle to travel by one wavelength *ß* under reference radiation force F_0 in a quasi-static state. For the case in panel (**a**), the trajectories occur over 0.13072 t_0 = 4s, with 1053 time steps taken during the simulation

Next, the agglomeration patterns of two to ten particles that are evenly spaced out on a circle in the pressure nodal plane are investigated. Figure 3 shows the initial (x, y) posi- tions of the particles in each case. In a plane standing wave, this scenario takes place when the PS particles are brought to the pressure node by the primary force. The particle tracing within the nodal plane allows demonstrating the formation of particle clusters under pure interaction forces, which is always attraction (Sepehrirahnama et al. 2015a, b; Doinikov 2001), since the primary force is zero on the pressure node. The particles were assumed to be Polystyrene (PS) beads in water. As expected, a pair of particles formed a dumbbell-shaped configuration. The three-sphere case resulted in a triangle-shaped cluster. For cases with more than 3 particles, the agglomeration pattern appears to be multiple layers of particles. It is concluded that particles tend to form large multi-layer agglomerates upon reaching the nodal plane.

Furthermore, particle aggregate undergoes rotation as it grows bigger and continues to rotate with respect to its center of mass after all the particles join in, as can be seen from their trajectories in Fig. 3. Observing the rotation of the aggregate was made possible by multi-particle tracing simu- lations of more than just 2 particles. The rotation occurred due to the component of the interaction forces orthogonal to the center-to-center line joining a pair of spheres in the sys- tem, which was reported in reference (Sepehrirahnama et al. 2015a, b). The agglomeration patterns of the five and six- particle cases are similar to those in Lim et al. (2019); Wang et al. (2017); Polychronopoulos and Memoli (2020), which reported the experimental study of the preferred agglomera- tion for acoustically levitated solid particles in air. In the supplementary video clips of reference (Lim et al. 2019), the aggregates slowly rotates with respect to its center of mass while individual particles fluctuate in the wave direction. It is noted that this rotation is primarily due to misalignment between the line of action of the acoustic interaction force and the centre-to-centre line of each pair in the aggregate (Sepehrirahnama et al. 2015a, b; Lopes et al. 2016; Doinikov 2001). While the rotation of such clusters appear in our simulation, this rotation was seldom observed in practical situations where a line of beads (pearl-chain configuration) emerges. This implies the possibility of other forces present in the system (such as acoustic streaming, friction, van der Waals forces) that may act on the particles.

In practical acoustofluidic devices with a rectangular channel and driven by ultrasound standing wave, a pearl-chain configuration of particles at the nodal plane was reported (Augustsson et al. 2012; Hartono et al. 2011; Mohapatra et al. 2018). However, our simulations so far showed that the line formation would be unlikely to occur if all the particles are initially on the nodal plane. To investi- gate the emergence of pearl-chain formation, we simulated the case of several particles positioned in a line formation on the nodal plane while another one approaches them from dif- ferent offsets in position, as shown in Fig. 4. It was observed that the pearl-chain configuration only occurs when all the particles lies within a plane parallel to the wave direction, as shown by the cases in the first column of Fig. 4. When the

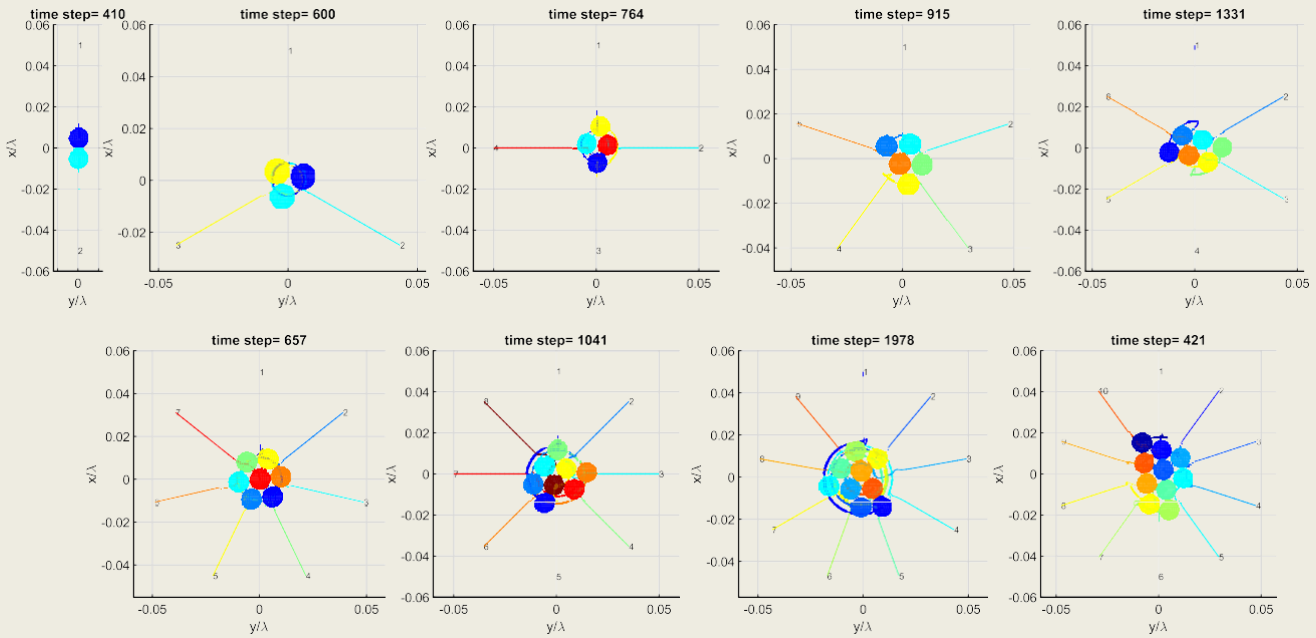

Fig. 3 Agglomeration patterns of two to ten-particle ensembles on the pressure node of a plane standing wave. Trajectories of particles are shown by the coloured lines

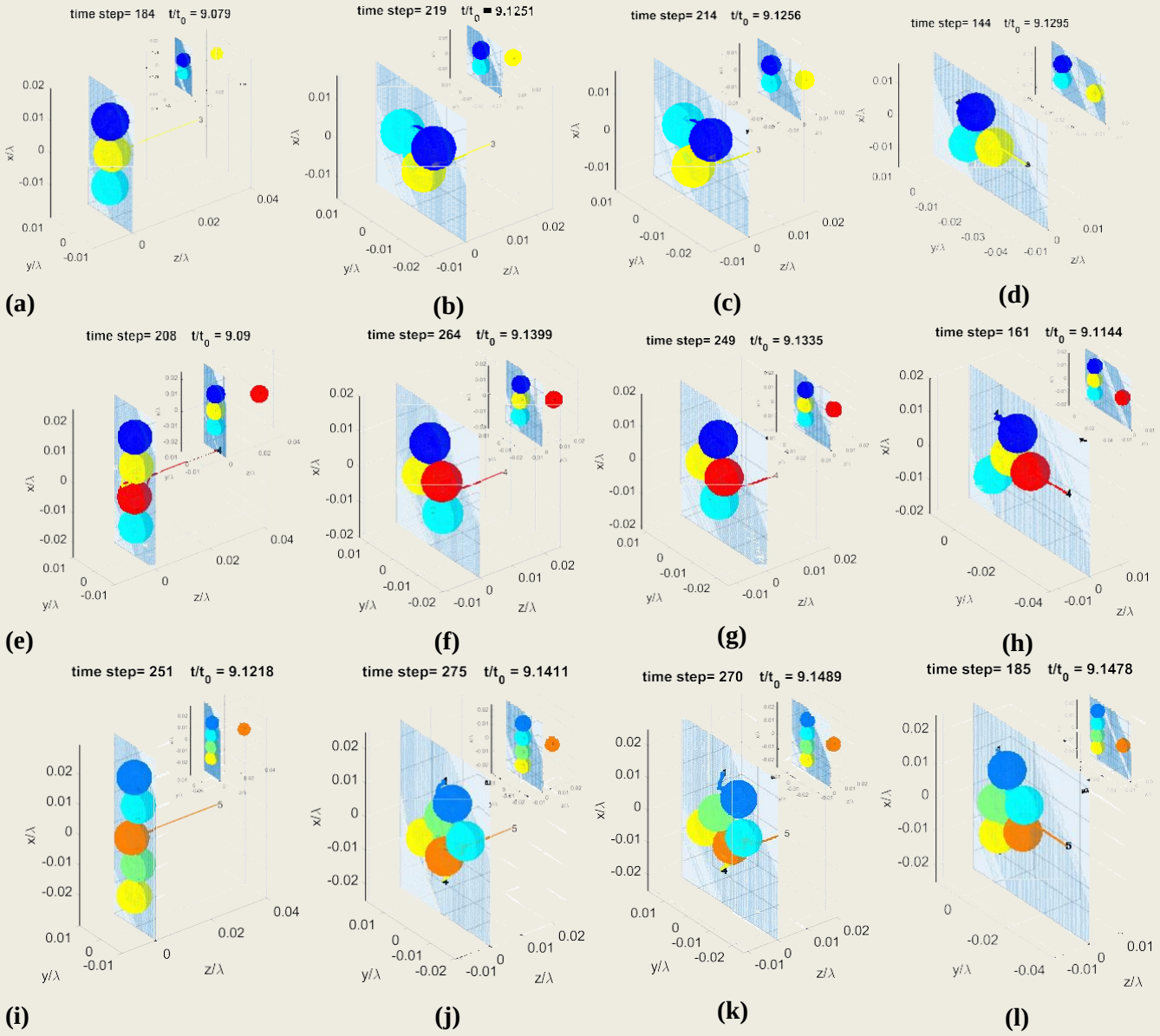

Fig. 4 Agglomerations of (**a**–**d**) three, (**c**–**h**) four and (**i**–**l**) five spheres under plane standing wave in the z-direction. In all these cases, one sphere is located initially away from others that form a line along the x-axis on the nodal plane. The sphere approaching the line aggregate is located about six times the radius away from the center of the aggregate with its position vector being at $0, \frac{\pi}{6}, \frac{\pi}{3}\ and\ \frac{\pi}{2}$ angle with respect to the z-axis

approaching sphere is offset from the existing pearl-chain, the pearl-chain will deform and interact with the approaching sphere, forming a layered structure which was observed in the last three columns of Fig. 4. Although our simulation results show that the pearl-chain or line configuration emerging from a random 3D distribution of particles is very unlikely, it has been yet reported in the experimental applications. This implies that, in practical applications, there should exist other weak forces due to factors such as sur- face finishing of the fluid-cavity walls or three dimensional resonance within the fluid cavity, as mentioned in reference (Mohapatra et al. 2018), that pushes particles into forming a pearl-chain configuration.

Finally, we look at the case of 20 rigid particles in the standing wave. The initial locations of these particles are in *x*-*z* plane and asymmetrically distributed at the vicinity of the pressure node. This case represents the situation in which the particles are brought to the vicinity of the nodal plane by the primary force and their relative distances are of the order of their diameters. Figure 5 shows their trajectories due to the acoustic forces. The particles form two separate clusters first at their own side before migrating together to

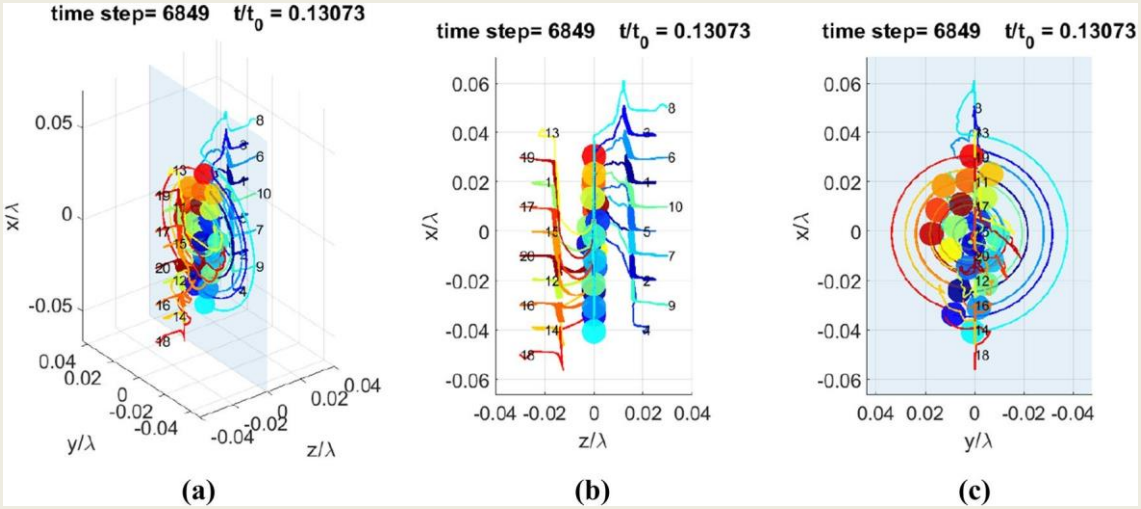

Fig. 5 a Isometric, **b** right and **c** front views of the trajectories of 20 particles in a standing wave along the *z* direction. The pressure node is illustrated by the transparent plane

the pressure nodal plane. It was observed that particles that were placed in *x*-*z* plane initially moved in the *y* direction due to the collective interaction forces acting upon each one of them. This phenomenon occurs due to the large number of particles and the strong attractive forces that brings particles towards the center of the cluster. Although the two-particle results seem very intuitive, the behavior of a large number of particle under acoustic forces is not easy to predict, since it largely depends on their initial positions and their interaction history along their paths.

3.1.1 Mixed solid-gas particle population

In some practical applications of sonocehmistry, particles with different materials coexist in a host fluid in addition to the bubbles that are generated by the ultrasound cavitation (Breen et al. 2001; Pol et al. 2003). Theoretical study of sub-wavelength air bubbles and solid particles showed that their interaction behavior is different from the case in which all the particles have the same material (Feng et al. 2020). However, that study was limited to the axisymmteric case of one solid particle and one bubble. To provide more physical insight about such interactions, we investigated the case of a single Polystyrene (PS) particle surrounded by air bub- bles in water. As shown in Fig. 6, all the air bubbles and PS particle were placed on the velocity node of a plane standing wave (denoted by V.N.), which is the natural agglomeration location for air bubbles. The PS bead experiences a zero primary force, but it is in an unstable equilibrium situation. The PS particle was placed at the center of the distribution in all cases. It was found that the bubbles attract each other strongly and subsequently push the solid particle to the outside of their aggregate. Although the PS particle, with a positive contrast factor, is in an unstable equilibrium in the velocity nodal plane, it is kept with the cluster of air bubbles due to the weak attractive interaction forces between the PS particle and the bubbles. Furthermore, the rotation of the aggregate that is entirely due to the multi-particle interactions was observed in these cases of mixed phases. These results show the significance of particle tracking simulations for understanding the physics of particle agglomeration in external acoustic fields. Our model of particle collision can be further improved by incorporating bubble coalescence and surface tension in future studies of bubble agglomeration by ultrasound.

For the case of one air bubble surrounded by PS beads on the velocity nodal plane, the agglomeration patterns are shown in Fig. 7. The initial arrangement of particles is the air bubble at the center and the PS beads are spaced out evenly in a circular pattern. It was observed that the air bubble remains at the center of the aggregate while attracting the PS beads. The attractive force between the air bubble and the PS bead is able to keep the PS beads at the velocity nodal plane that is otherwise an unstable equilibrium location for the beads. The arrangement of the solid spheres in the final configuration is symmetric with respect to the air bubble at the center. These agglomeration patterns are different from the case of multiple bubbles and a single solid particle, in which the solid particle is pushed away from the center of the aggregate to the outside due to the stronger interaction forces between bubbles. The rotation of the aggregate was also observed for this case.

The variety in the patterns of particle agglomeration under plane standing wave shows the level of complexity of multiple interactions as the number of particles grow. It also implies the limitations of the two-particle models such

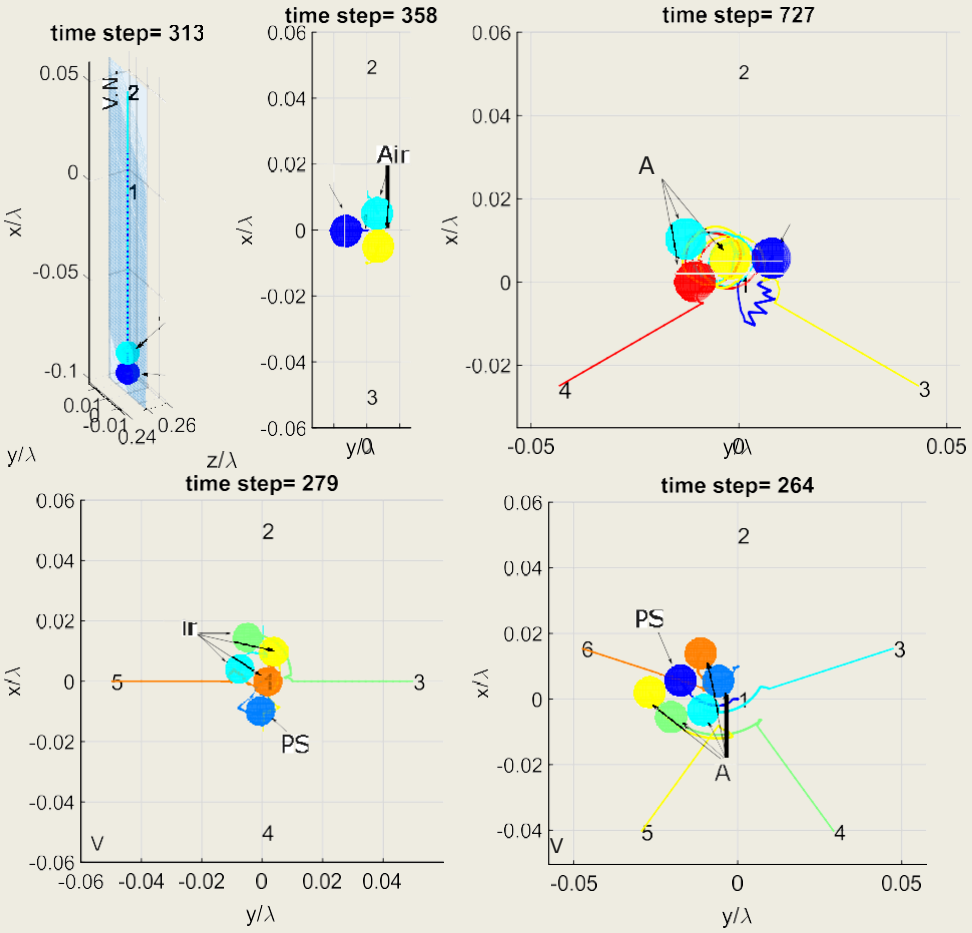

Fig. 6 Agglomeration behavior of air bubbles around a single Polystyrene bead of the same size in water in a plane standing wave

as solid-solid (Sepehrirahnama et al. 2015a, b; Doinikov 2001; Silva and Bruus 2014) or solid-bubble interactions (Doinikov 2001, 2002; Feng et al. 2020). And finally, to complete those models, the hydrodynamic drag forces and the collision between the particles should be accounted for.

3.2 Bessel standing wave

A Bessel standing wave along the z-axis is considered. The incident wave with the cone angle of $\frac{\pi}{3}$ is illustrated in Fig. 8a. The pressure nodes in the cylindrical radius R direction are marked by red circular lines, while the black lines show the velocity nodes. These radii of the red and black rings are the roots of J_0 and J_1, respectively. The pressure node in the z direction is illustrated by the green-shaded slice (denoted by P.N.) at $z = 0$. The particle tracking has been performed for 20 spherical particles. The simulations were conducted with the particles placed near three equilibrium locations in the field: at the axis $R = 0$ (also the first root of J_1), first pressure nodal circle (ring 1 which is the first root of J_0), and the first velocity nodal circle (ring 2 which is the second root of J_1). For the first case, the ensemble is placed near the wave axis within P.N., as shown in Fig. 8b. From the initial configuration ($t = 0$), after some time, they formed an elongated aggregate along the axis, as $R = 0$ is a line of equilibrium for the particles. It was found that the elongated structure formed by the spheres also rotates with respect to its center of mass, similar to the case of plane standing wave. In the second case, the ensemble of particles is placed in the vicinity of the ring 1, which is one of the unstable equilibrium locations in the primary force field, as shown in Fig. 8c. The particles in the inner side of the ring experience a larger acoustic force and are pushed away faster. They also form small clusters due to the interaction forces among themselves while moving away. Particles that are initially located on the ring were knocked out of their positions by the interaction forces, even though the primary force is zero there, implying the instability of their resting state on this pressure node. In the last case, as shown in Fig. 8d, the agglomeration pattern near ring 2 was investigated. The particles are expected to spread and form an arc along the ring due to the primary forces; however, their interactions cause them to form several layers on top of each other with the center of mass of the aggregate being located on the inner

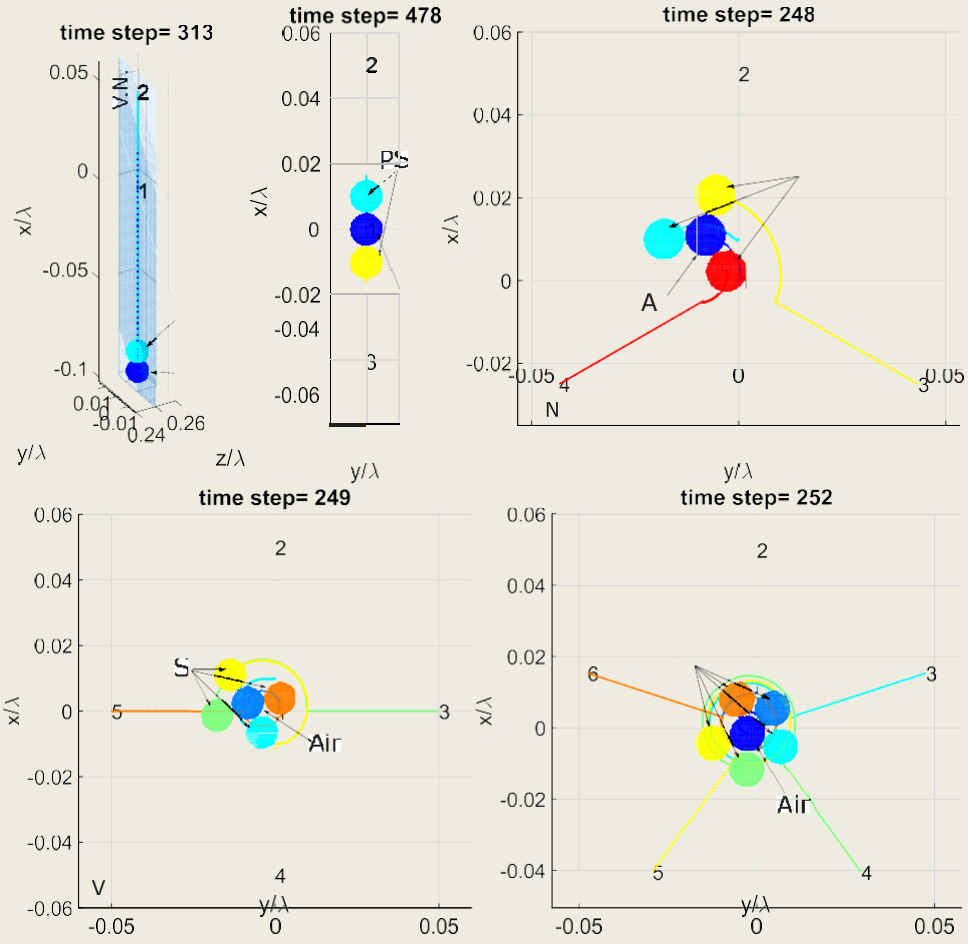

Fig. 7 Agglomeration behavior of Polystyrene beads around a single air bubble of the same size in water in a plane standing wave

0

side of the ring. The observed modes of agglomeration in the field of Bessel standing wave demonstrate the promising aspect of of the non-planar pressure fields for designing targeted particle manipulation using ultrasound.

4 Discussion

Particle tracking simulation under a force field needs an algorithm for collision detection and a rule for adjusting the size of time increment. In the proposed model, the displacement magnitude of the particle with the largest velocity is limited to 45% of its radius prior to applying the position correction technique for colliding particles. This provides an adaptive time stepping scheme where the step size is determined by the largest velocity within each time step. To illustrate this, the evolution of time increment and magnitude of displacement are shown in Fig. 9 for the case of three spheres in a plane standing wave. Two of the spheres are initially on the pressure nodal plane (P.N.). Due to the stronger interaction, these two come in contact first at time step 5, as shown in Fig. 9a. The blue sphere joins the other two spheres after some time at time step 37. Before time step 5, the size of the time increment was determined by the velocity of sphere 3, shown with the yellow color, since it was moving faster. After the first collision, the time increment is determined by the velocity of sphere 1, shown with the blue color. The time increment reduces to about 25% of its largest value at time step 3 and remains at that level for the rest of time steps, which allows the next possible collisions to be captured automatically in our algorithm. The displacements of sphere 2 and 3 after the first collision is the same since they remain as an entity before sphere 1 joins them at time step 37. Although the performance of the proposed algorithm was shown for spherical particles, our adaptive algorithm is applicable to non-spherical shapes of particles as long as their displacements are constrained to a fraction of their characteristic sizes, in such as way that no collision event is missed out.

Applying the position correcting technique adds to the computational cost of particle tracking simulation. To investigate the computational complexity of the present algorithm, several configurations of particles in which each particle is in contact with at most 4 others on the pressure

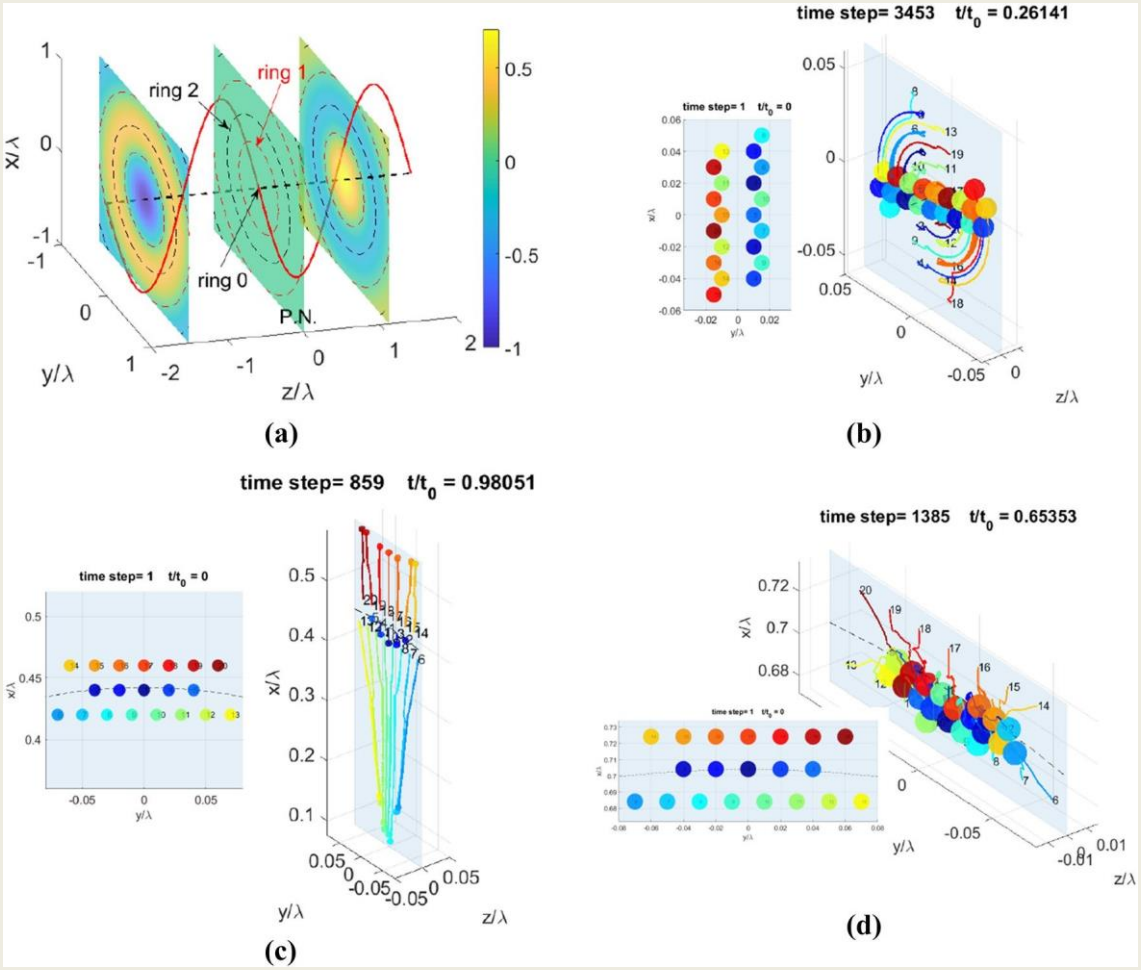

Fig. 8 a Incident potential field of a standing Bessel beam with the cone angle of $\frac{\pi}{3}$ and the axis, shown as dotted line, along the z direction, and the trajectories of 20 rigid particles initially positioned around **a** ring zero (kR = 0), **b** ring one (kR = 2.78) that indicates the first root of J_0, and **c** ring two (kR = 4.42) that indicates the second root of J_1

node in a plane standing wave were considered. The computation time of imposing the no-penetration constraint using the proposed algorithm was measured with respect to the number of particles, as shown in Fig. 10. This is the CPU time of running our C++ implementation of the algorithm for one time-step of particle tracking simulation on a Desk- top Workstation with Intel Xeon CPU running at 3.6 GHz, 32 GB of RAM and 64-Bit Windows 10. From the trend of data points, it was found that the computational complexity of the presented algorithm is of the order of $\vartheta(N^{2.37})$. It is smaller than the computational cost of solving the coupled multi-scattering wave problem and hydrodynamic interaction problem when the particles are close to each other; both problems have a computational complexity of order $\vartheta(N^3)$. Furthermore, it was found that the arrangement of the spheres prior to applying the contact algorithm affects the computation time, causing a non-uniform trend instead of a monotonic increase. Nevertheless, applying the contact algorithm is absolutely necessary for such simulations of particulate systems under an external force field.

The present model can be further improved for simulating bubble-bubble interactions, coalescence and shape deformation during their motion under acoustic radiation forces, by adding surface tension, internal pressure and solving multiple scattering problem using numerical methods such as Boundary Element Method. The present model assumed sufficiently weak incoming and scattered waves, where the total first-order acoustic field is given by the linear superposition of the incident and scattered fields from all spheres. Such a model is valid for cases where the deformation of the spheres is small, such as microfluidic applications with biological cells and polystyrene beads reported in the literature. When there is significant deformation of the spheres in the presence of strong waves, an iterative scheme will have to be used to solve the nonlinear problem. Although the individual size of particles are within Rayleigh limit in

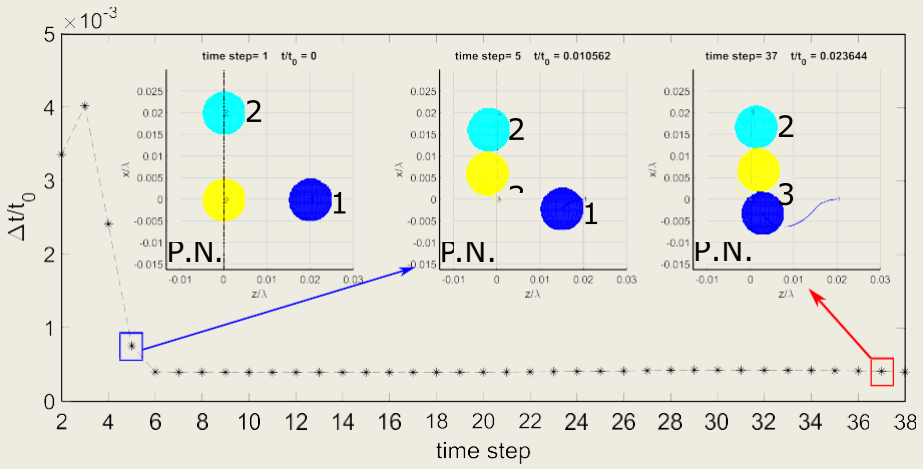

(a)

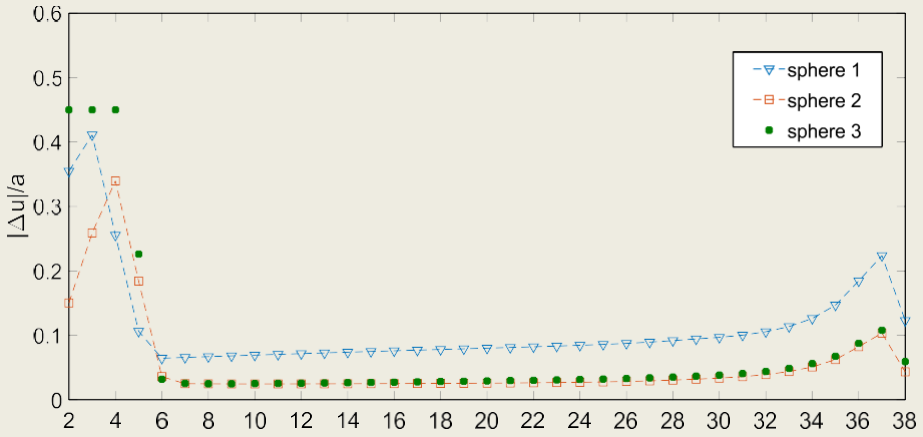

(b)

Fig. 9 Evolution of (**a**) the time increment *At* and (**b**) the displacement magnitude ***Au*** during the particle tracking for three spheres of the same size in a plane standing wave

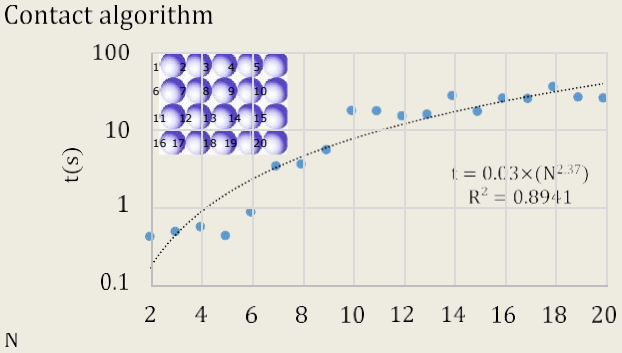

Fig. 10 Computation time of contact algorithm in seconds with respect to the total number of spheres *N*

the presented results, their cluster size could grow beyond this limit. Our model is still applicable by including more terms from the multipole series expansions Eqs. (4) and (5) to capture the near-field scattering effects, resulting in more accurate estimate of the acoustic radiation forces during the agglomeration of a large population of particles. However, adding more terms in the multi-scattering simulation is computationally more expensive. Further improvements are required to include surface effects such as van der Waals forces, friction or interactions of electromagnetic type. The effects of nearby walls may also be included for more realis- tic situations in microdevices, as the present model assumed an infinite fluid domain. The host fluid was assumed to be a non-viscous medium, meaning that wave attenuation and acoustic streaming effects were neglected too. Including such viscosity effects requires significant improvement of this model (Sepehrirahnama et al. 2015a, b, 2016). Nonetheless, it can be used for modelling agglomeration of spherical particles in fluids with negligible viscosity.

Lastly, the cluster patterns obtained from our simulations match well with reported experiments in the literature (Lim et al. 2019; Wang et al. 2017). Similar patterns of parallelogram and chevron shapes were seen within the nodal plane for five and six particles in a cluster. While good qualitative agreement can be seen, detailed matching in particle

trajectory is difficult as detailed and precise information, such as the entire 3D pressure field, distribution of acoustic energy density, initial positions and velocities of the particles, are required. In some studies that dealt with the levitation of a small population of particles (Lim et al. 2019; Wang et al. 2017; Polychronopoulos and Memoli 2020), these information were missing and only qualitative comparison was possible.

5 Conclusion

Particle cluster formation under planar and non-planar standing waves was investigated. A theoretical model was proposed for particle tracking under the influence of acoustic and hydrodynamic forces, and taking into account collision. The model was first used to simulate a pair of particles under a plane standing wave. It was shown that the inter-particle interactions become important when they are close to each other at the vicinity of the pressure nodal plane. In a mixture of bubble and solid particles, solid particles are kept on the velocity nodal plane, which is their natural unstable equilibrium location, due to the interaction between them and the bubbles. The particle aggregates also go under rotation due to the resultant interaction torque. The possibility of pearl-chain configuration emerging in a plane standing wave was shown to be very low theoretically, which is in contrast with the experimental observations. We also showed that the proposed model is scalable by simulating a non-symmetric distribution of twenty particles around the pressure node.
Using two zero-order Bessel beams propagating in oppo- site directions, a Bessel standing wave was generated in the z direction. A population of twenty particles, distributed around the Bessel function wavefront in the x-y plane, was simulated using the particle-tracking model. It was shown that agglomeration patterns under the Bessel standing wave depend on the initial locations of the particles with respect to the beam axis. These patterns emerge as a result of the non-planar distribution of pressure wave-front, unlike the case of plane standing wave where particles can roam around on the nodal plane. The present agglomeration patterns in planar and non-planar standing waves show that there is a potential for designing particle-manipulation processes by ultrasound, such as air bubbles in the sonochemistry applications, based on theoretical modeling and simulation.

Acknowledgements This work was supported by the Ministry of Education, Singapore, through the National University of Singapore, Faculty of Engineering (Tier 1 Grant R-265-000-652-114).

Compliance with ethical standards

Conflict of interest The authors declare that they have no conflict of interest.

References

Augustsson P, Magnusson C, Nordin M, Lilja H, Laurell T (2012) Microfluidic, label-free enrichment of prostate cancer cells in blood based on acoustophoresis. Anal Chem 84(18):7954
Breen M, Dinsmore A, Pink R, Qadri S, Ratna B (2001) Sonochemically produced ZnS-coated polystyrene core- shell particles for use in photonic crystals. Langmuir 17(3):903
Chen Y, Truong VN, Bu X, Xie G (2020) A review of effects and applications of ultrasound in mineral flotation. Ultrason Sono- chem 60:104739
Devendran C, Gralinski I, Neild A (2014) Separation of particles using acoustic streaming and radiation forces in an open micro- fluidic channel. Microfluidics Nanofluidics 17(5):879
Doinikov AA (1994a) Acoustic radiation pressure on a rigid sphere in a viscous fluid. Proc R Soc Lond Ser A 447(1931):447
Doinikov AA (1994b) Acoustic radiation pressure on a compressible sphere in a viscous fluid. J Fluid Mech 267:1
Doinikov AA (1999) Bjerknes forces between two bubbles in a vis- cous fluid. J Acoust Soc Am 106(6):3305
Doinikov AA (2001) Acoustic radiation interparticle forces in a compressible fluidm. J Fluid Mech 444:1
Doinikov AA (2002) Viscous effects on the interaction force between two small gas bubbles in a weak acoustic field. J Acoust Soc Am 111(4):1602
Doinikov AA, Combriat T, Thibault P, Marmottant P (2016) Effect of surface waves on the secondary Bjerknes force experienced by bubbles in a microfluidic channel. Phys Rev E 94(2):023105
Feng K, Wang C, Mo R, Hu J, Li S (2020) Interaction between particles and bubbles driven by ultrasound: Acoustic radiation force on an elastic particle immersed in the ideal fluid near a bubble. Ultrason Sonochem 67:105166
Garcia-Sabaté A, Castro A, Hoyos M, González-Cinca R (2014) Experimental study on inter-particle acoustic forces. J Acoust Soc Am 135(3):1056
Hartono D, Liu Y, Tan PL, Then XYS, Yung LYL, Lim KM (2011) On-chip measurements of cell compressibility via acoustic radiation. Lab Chip 11(23):4072
King LV (1934) On the acoustic radiation pressure on spheres. Proc R Soc Lond Ser A 147(861):212
Lei J (2017) Formation of inverse Chladni patterns in liquids at microscale: roles of acoustic radiation and streaming-induced drag forces. Microfluidics Nanofluidics 21(3):50
Lim MX, Souslov A, Vitelli V, Jaeger HM (2019) Cluster formation by acoustic forces and active fluctuations in levitated granular matter. Nat Phys 15(5):460
Lopes JH, Azarpeyvand M, Silva GT (2016) Acoustic interaction forces and torques acting on suspended spheres in an ideal fluid. IEEE Tran Ultrason Ferroelectr Freq Control 63(1):186
Ma X, Huang B, Wang G, Zhang M (2017) Experimental investiga- tion of conical bubble structure and acoustic flow structure in ultrasonic field. Ultrason Sonochem 34:164
Marston PL (2006) Axial radiation force of a Bessel beam on a sphere and direction reversal of the force. J Acoust Soc Am 120(6):3518
Marston PL (2007) Axial radiation force of a Bessel beam on a sphere, direction reversal of the force, and solid sphere exam- ples. J Acoust Soc Am 121(5):3109
Marston PL, Wei W, Thiessen DB (2006) Acoustic radiation force on elliptical cylinders and spheroidal objects in low frequency standing waves. AIP Conf Proc 838:495–499
Mishra P, Hill M, Glynne-Jones P (2014) Deformation of red blood cells using acoustic radiation forces. Biomicrofluidics 8(3):034109 Mitri F (2015) Acoustic radiation force on oblate and prolate spheroids in Bessel beams. Wave Motion 57:231

Mohapatra AR, Sepehrirahnama S, Lim KM (2018) Experimental measurement of interparticle acoustic radiation force in the Ray- leigh limit. Phys Rev E 97(5):053105
Pol V, Gedanken A, Calderon-Moreno J (2003) Deposition of gold nanoparticles on silica spheres: a sonochemical approach. Chem Mater 15(5):1111
Polychronopoulos S, Memoli G (2020) Acoustic levitation with opti- mized reflective metamaterials. Sci Rep 10(1):1
Pozrikidis C et al (1992) Boundary integral and singularity methods for linearized viscous flow, boundary integral and singularity methods for linearized viscous flow. Cambridge University Press, Cambridge
Sepehrirahnama S, Lim KM (2020) Generalized potential theory for close-range acoustic interactions in the Rayleigh limit. Phys Rev E 102:043307
Sepehrirahnama S, Lim KM, Chau FS (2015a) Numerical study of interparticle radiation force acting on rigid spheres in a standing wave, numerical study of interparticle radiation force acting on rigid spheres in a standing wave. J Acoust Soc Am 137(5):2614
Sepehrirahnama S, Lim KM, Chau FS (2015b) Numerical analysis of the acoustic radiation force and acoustic streaming around a sphere in an acoustic standing wave. Phys Proced 70:80
Sepehrirahnama S, Chau FS, Lim KM (2016) Effects of viscosity and acoustic streaming on the interparticle radiation force between rigid spheres in a standing wave. Phys Rev E 93(2):023307
Settnes M, Bruus H (2012) Forces acting on a small particle in an acoustical field in a viscous fluid. Phys Rev E 85(1):016327
Shang X, Huang X, Yang C (2016) Bubble dynamics in a microfluidic chamber under low-frequency actuation. Microfluidics Nanofluid- ics 20(1):14
Silva GT, Bruus H (2014) Acoustic interaction forces between small particles in an ideal fluid. Phys Rev E 90(6):063007
Tiong TJ, Chu JK, Lim LY, Tan KW, Yap YH, Asli UA (2019) A com- putational and experimental study on acoustic pressure for ultra- sonically formed oil-in-water emulsion. Ultrason Sonochem 56:46
Vyas V, Lemieux M, Knecht DA, Kolosov OV, Huey BD (2019) Micro- Acoustic-Trap (μAT) for microparticle assembly in 3D. Ultrason Sonochem 57:193
Wang M, Qiu C, Zhang S, Han R, Ke M, Liu Z (2017) Sound-medi- ated stable configurations for polystyrene particles. Phys Rev E 96(5):052604
Wijaya FB, Lim KM (2016) Numerical calculation of acoustic radiation force and torque on non-spherical particles in Bessel beams. Proc Meet Acoust 17IASA 26:045002
Wijaya FB, Mohapatra AR, Sepehrirahnama S, Lim KM (2016) Cou- pled acoustic-shell model for experimental study of cell stiffness under acoustophoresis. Microfluidics Nanofluidics 20(5):69
Wiklund M (2012) Acoustofluidics 12: biocompatibility and cell viabil- ity in microfluidic acoustic resonators. Lab Chip 12(11):2018
Wiklund M, Green R, Ohlin M (2012) Acoustofluidics 14: applica- tions of acoustic streaming in microfluidic devices. Lab Chip 12(14):2438
Xuan X, Zhu J, Church C (2010) Particle focusing in microfluidic devices. Microfluidics Nanofluidics 9(1):1
Yosioka K, Kawasima Y (1955) Acoustic radiation pressure on a com- pressible sphere. Acta Acust United Acust 5(3):167
Zhang Y, Li S (2016) The secondary Bjerknes force between two gas bubbles under dual-frequency acoustic excitation. Ultrason Sono- chem 29:129
Zhang L, Marston PL (2011) Geometrical interpretation of negative radiation forces of acoustical Bessel beams on spheres. Phys Rev E 84(3):035601

VI. PRODUCTS AND SERVICES FROM OUR MEMBERS

ACOUSTICS AND VIBRATION CONSULTING MALAYSIA (AVCM) SDN. BHD.

Acoustics and Vibration Consulting Malaysia (AVCM) Sdn. Bhd. is an acoustical company based in Kuala Lumpur, Malaysia, also a member of *Geonoise Asia Co. Ltd*. AVCM specializes in the noise and vibration field, striving to improve the environmental quality,

specifically on noise, by providing relevant services and solutions to customers. Our services and products include:

- Acoustical Consultation - Geonoise
- Calibration Products - SPEKTRA
- Noise Modelling Software - SoundPLAN
- Vibration Monitoring System & Pile Integrity Testing - Profound
- Acoustical Insulation Calculation - SONarchitect ISO
- Noise & Vibration Sensors/Instruments - PLACID Instruments
- Acoustics & Audio Measurement Instruments - Bedrock
- Analysis of Sound in Duct Networks - SIDLAB
- Noise & Vibration Testing & Data Acquisition - m+p
- Smart Noise & Vibration Excitation Technology – Qsources

For more details on the software/hardware we have, do take a look at our company's website. We are also reachable through LinkedIn and Facebook.

Calibration with AVCM

CV -10, a one stop solution for on-site calibration.

That is right! The CV-10 is a mobile vibration calibrator by SPEKTRA, suitable for calibration of accelerometers, proximity, and vibration velocity sensors and many more. The frequency range of CV-10 covers the range of 5 Hz to 10 kHz, with maximum acceleration of 200 m/s^2. Its internal rechargeable battery allows an operation of up to 10 hours and is stored in a rugged case for daily on-site operation. Another bonus feature of CV-10 is the Easy Data Exchange function via USB, with an optional choice of having Ethernet/Wi-Fi connections.

For more details, visit our CV-10 product page: https://avcm.my/cv-10/

Acoustic Camera

The **Norsonic Hextile** is a module-based approach to acoustic camera that gives the user both portability and great resolution for a wide range of measurement situations. The array dish is based on a hexagon shape, given it both its name, and the ability to combine several tiles into larger systems.

With Hextile, user has a *small, portable and lightweight* acoustic camera to be used for a wide range of measurement situations. There is a USB connection for both power and data transfer, hence no extra battery cable is required. This array is made from aluminium, which is robust and lightweight, containing 128 MEMS microphones, but still less than 3kg while having a maximum diameter of 46 cm. The Hextile has a low frequency limit of 410 Hz.

To learn more about Norsonic Hextile, visit the Norsonic's page: https://web2.norsonic.com/product_single/acoustic-camera/

VI. ACOUSTICAL NEWS

The National Environmental Agency of Singapore has launched a SGD 2 million new foundation to further encourage construction companies to use machineries with lower noise levels to provide a more quiet and pleasant living environment.

This new fund entitled Quieter Construction Innovation Fund will be for a period of two years and will replace the current Quieter Construction Fund which will expire on 31 March 209. This new fund will assist construction companies to purchase , rent machineries or to use new methods to reduce the noise generated during construction and to enable the nearby residents to enjoy a more peaceful living environment.

The local construction companies can begin to apply for this fund from 1 April 2019 onwards. Each application is capped at

three hundred thousand Singapore dollars. It will be different from the current framework. Those applying for reducing piling noise and demolition noise equipment and can have maximum eight thousand Singapore dollars assistance for application under two hundred Singapore dollars. For application exceeding half a million Singapore dollars will have a maximum three hundred thousand dollars subsidies. The condition is that these noise reducing equipment must be able to produce a 10 decibels noise reduction.

To rent piling and demolition noise reduction equipment and materials can be entitled to a nine thousand to fifty thousand Singapore dollars assistance.

Up to end of February 2019, the current Quieter Construction Fund has approved 126 applications and provided a total of 5.1 millions dollars to 112 construction sites. It is anticipated that by the expiry of this fund, the total fund allocated will reach a level of 7.5 million dollars.

VI.REPORT ON CONFERENCES

The Regional Conference on Acoustics and Vibration (RECAV) organised by the Society of Acoustics(Singapore) and the Association of Acoustics and Vibration Indonesia(AAVI) was successfully held in Bali,Indonesia from 27 to 28 Nov 2017. There were 110 presentations from 14 countries with 60% of them from Indonesia. There were also some 18 exhibition booths. This reflected strong local participation and the international nature of the conference.

VII. BID FOR FUTURE INTERNATIONAL CONFERENCES

The Society of Acoustics(Singapore) will be hosting the ICSV28 in Singapore from 24 to 28 July 2022 at the Marina Bay Sands Hotel.

Government Bodies

www.mom.gov.sg

www.nea.gov.sg

www.lta.gov.sg

Technical and Research Sites

Corporate Sites

www.metaultrasound.com

www.noisecontrols.com

(The Society welcomes interested parties to contribute relevant websites to the above e useful links. For more information, please contact us. Thank you.)

Society of Acoustic, be liable for any collateral, special or consequential damage as a result of the use of the information contained in the article.

President: Woon Siong Gan

E-Newsletter compiled by: Woon Siong Gan